Feedback-Controlled Flux Modulation for High-Temperature Superconducting Magnets in Persistent Current Mode

Muhammad Iftikhar, Min Zhang, Weijia Yuan

Applied Superconductivity Laboratory, Department of Electronic and Electrical Engineering University of Strathclyde, G1 1XW Glasgow. United Kingdom.

E-mail: min.zhang@strath.ac.uk

December 2022

Abstract. High-temperature superconducting (HTS) magnets have found wide applications in high-field settings owing to their high current capabilities. Typically, these magnets are powered by high-current power supplies via current leads, which can complicate insulation between cryogenic and room temperature environments. However, new developments in flux pumps for HTS magnets have enabled charging of kA levels of current without power supplies. By combining flux pumps with HTS persistent current operation, it is possible to achieve accurate flux modulation and eliminate the need for power supplies and current leads. In this study, we report on a novel feedback-controlled flux modulation for HTS magnets in persistent current operations. This flux modulation is based on a flux pump mechanism that generates a DC voltage across the charging superconductor by applying a current higher than its critical current. With closed-loop feedback control, our flux modulation can achieve precise injection and reduction of HTS magnet current in increments of 0.5 A. This technology can lead to stable magnetic fields in HTS magnet designs. We anticipate that this work will enable future magnets to operate in a stable persistent current mode within a closed cryogenic chamber, significantly reducing the footprint and power demand of HTS magnets and opening up new opportunities for their applications.

1. Introduction

Superconducting technology has evolved over time, resulting in a wide range of industrial applications and commercial products. For instance, magnetic resonance imaging (MRI) and nuclear magnetic resonance (NMR) machines use superconducting magnets to generate the necessary magnetic fields [1–4]. These machines are essential for modern medical diagnosis [3, 5]. Advancements in the manufacturing of high-temperature (HTS) coated conductors (CCs) [6–8] have made it possible to produce long, robust HTS-CCs with bending tolerance suitable for winding superconducting coils. As a result, HTS coils have become a competitive option for high magnetic field applications [3, 4].

HTS-CC magnets are unmatched in their ability to generate strong, uniform, and ultra-stable magnetic fields. These advantageous properties result from confining supercurrents to

high inductance coils with extremely low operational resistance. Studies have shown almost negligible attenuation, with the magnetic field produced sustained to better than 1 ppbh^{-1} in some cases, and extremely large decay times [9]. These so-called persistent mode-driven electromagnets transform into the world's highest field quasi-permanent magnets. Persistent current operation in an HTS coil becomes possible by including an HTS persistent joint in the circuit. Ohki et al. (2017) presented an intermediate grown superconducting (iGS) joint between REBCO coated conductors and achieved a joint resistance of $< 5\times10^{-13} - 3\times10^{-12}$ Ω [10]. It has also been observed that in the iGS joints between REBCO coated conductors, the critical current degrades to 45% of the coated conductor critical current at 77K in a self-field with a criteria of 1μV. Recently, Yanagisawa et al. (2021) used an iGS superconducting joint between coated conductors in their persistent-mode NMR magnet, achieving temporal stability of ∼1ppm [11]. This allowed for high-resolution NMR spectra to be obtained using a dc source and thermal switches (heaters) for charging the coil. In addition to a superconducting joint, Lee et al. (2013) presented a wind-and-flip method to achieve a jointless HTS coil and demonstrated persistent current operation with zero field cooling [12].

A natural question that arises here is how HTS coils are energized. There are two possible options for energizing an HTS coil: direct current injection and indirect current induction. In direct current injection, the coils are connected to a power supply and energized through current leads [13]. This approach can be problematic, especially for high-current applications, because the current leads needed to transmit very high currents are extremely bulky, such as in the W7-X project, where 17.6 kA is required [14, 15]. More importantly, the current leads create a path between the cryostat (cold) and the room temperature environment, imposing a heavy thermal load on the cooling systems [16–18] and resulting in significant additional capital and operating costs [19]. An alternative solution for indirect current induction is to incorporate a flux pump, which can constantly drive magnetic flux into a closed superconducting circuit without physical connections [20–32]. The flux pumping effect was originally discovered for low-temperature superconductors (LTS) [33–42]. It was later discovered that eliminating superconductivity is not necessary for high-temperature superconductors, leading to the new era of HTS flux pumps. Various developments in HTS flux pumps have been reported recently. These flux pumps include traveling magnetic field-induced flux pumps (dynamo, linear flux pumps) [22, 24, 43–45] and HTS rectifier flux pumps (thermally switching, dynamic resistance switching, JcB switching, and self-switching) [26–28, 46–48]. HTS flux pumps can charge the magnet and compensate for any current decay, enabling the quasi-persistent operation of HTS-CC magnets. The contact voltage drop of soldering joints is considerably less than the voltage determined from the *E-J* relationship and is therefore considered negligible. The resistance of soldering joints still does not diminish to zero, so the current flowing through HTS magnets will still decay over time. In [49], a ring-shaped HTS magnet with a trapped field of 4.6 T after field cooling magnetization at 25 K is reported. This magnet can be operated in persistent current mode, but it will be difficult to compensate for the current decay when exposed to an external AC magnetic field without continuous charging using a flux pump. To date, it is still challenging to keep an HTS magnet working in a persistent current mode without soldering joints, and it

requires continuous current injection with a flux pump.

This paper proposes a novel closed-loop feedback control for charging high-temperature superconducting (HTS) magnets in persistent current operations. Closed-loop feedback control is widely used in many engineering applications, including motor drives [50], the motion of atoms in optical cavities [51], and stabilizing Rabi oscillation in superconducting qubits [52]. In an HTS coated conductor (HTS-CC), flux flow resistivity appears when there is flux motion. This phenomenon occurs when a superconductor is subjected to an AC field, transporting an AC current or a DC current above its critical current value. In [43], the authors proposed a self-switched HTS flux pump that works by driving the HTS-CC into the flux flow region on the *E-J* curve by injecting current above its critical current value. Building on this initial work, this paper presents a closed-loop feedback control system to induce a flux flow voltage and achieve bidirectional current control for an HTS coil in persistent current operation. The feedback control allows for effective flux modulation by accurately injecting and removing current in an HTS magnet, enabling precise field control of the magnet.

2. Closed-Loop Feedback Control

Closed-loop control systems are desirable in systems that are more sensitive to disturbances because of their ability to modify the natural dynamics of a system and stabilize it, which is a key feature of any closed-loop system. In contrast, open loop systems, such as previously reported flux pumps, do not have control over the current state of the system. In the closed-loop control system described here, the set point for the required magnetic field is assigned, and the error between the magnet current and the set point is obtained. Based on the magnitude of the error, a control block calculates the required voltage and corresponding current needed to charge the magnet. This current value is then fed to a limit block that is in place to protect the HTS-CC from quenching; in this case, the limit is set to be 140% of the critical current of the HTS bridge. The signal generation block generates an analogue signal based on the current value, which is fed into an amplifier. The amplifier is connected to the primary of the transformer, inducing the charging current on the secondary coil. When the charging current exceeds the critical current of the bridge, a voltage appears across the bridge, causing flux pumping into the HTS magnet.

The block diagram in Figure 1 illustrates the proposed closed-loop feedback control HTS flux pump. The control algorithm, implemented using LabVIEW, estimates the required voltage for injecting flux into the HTS magnet and generates an input signal for the primary of the transformer to achieve flux pumping. In self-switching HTS flux pumps, the flux injection is achieved by driving the superconductor into the mixed state, but the non-linear $V-I$ characteristics at this state can present a difficulty in accurately estimating and controlling the flux injected into the HTS magnet. Our results show that this difficulty can be overcome through the use of the proposed control system.

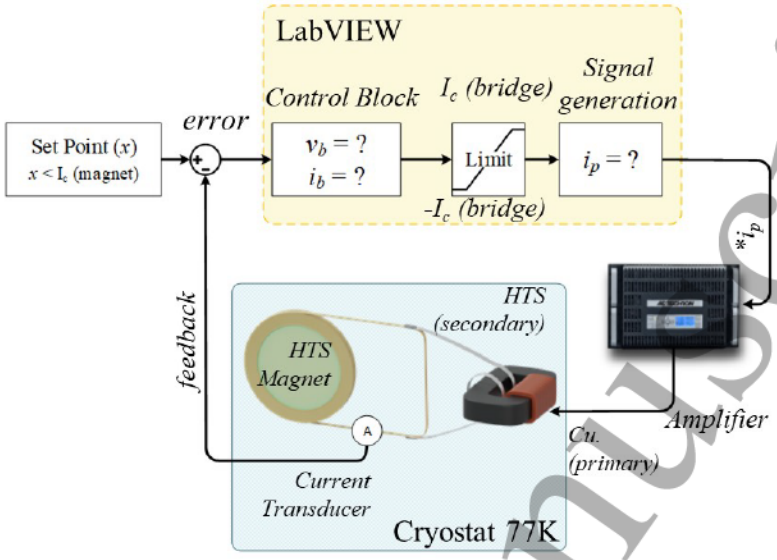

Figure 1: Block diagram of the closed-loop feedback control system for HTS magnets. The control algorithm, implemented in LabVIEW, determines the required voltage for injecting flux into the magnet and generates an appropriate input current for the flux pump. It also continuously monitors the current flowing into the load magnet and calculates the error for the next iteration.

2.1. Voltage Prediction in High Temperature Coated Conductors

To predict the voltage across an HTS coated conductor in the mixed state, the structure of the conductor must be taken into account. Second generation (2G) HTS conductors are composed of multiple layers, including a high-temperature superconducting layer, a substrate (Hastelloy) layer, a buffer stack layer, two silver overlays, and two electroplated copper layers [53]. The resistivity of the metal layers is well-known, but the resistivity of the HTS layer can be characterized using the $E-J$ Power Law.

$$\rho_{hts}(I_c) = \frac{V_c}{I_c} \times \left(\frac{I_T}{I_c}\right)^{n-1} \tag{1}$$

Where, ρ_{hts} is resistivity of HTS layer, V_c is voltage criterion 10^{-4}V, I_c is critical current of HTS tape, I_T is the transport current, and n is the exponent of power law. As the transport current exceeds the critical current value of the superconducting layer (YBCO), it enters the mixed state (flux flow regime) and redistributes itself to other metal layers [54]. The net voltage due to flux flow resistivity can be calculated using the following formula:

$$\frac{V}{l} = I_T \cdot \frac{\rho_{hts} \cdot \rho_{layer}}{\rho_{layer} \cdot S_{hts} + \rho_{hts} \cdot S_{layer}}$$

$$\frac{R_{ff}}{l} = \frac{\rho_{hts} \cdot \rho_{metal}}{\rho_{metal} \cdot S_{hts} + \rho_{hts} \cdot S_{metal}} \tag{2}$$

Where R_{ff} is flux flow resistance, ρ_{hts} is resistivity of HTS layer, S_{hts} is cross-sectional area of HTS layer, ρ_{layer} is resistivity of metal layers, S_{layer} is cross-sectional area of metal layers and l is the length of the HTS tape. In equation 2 the resistivity of the metal layers is known [55, 56] except the YBCO layer. Assuming the current density and electric field to be uniform across the length (l) of HTS tape, the electric potential and current density of an HTS tape can be derived as;

$$| E(t) | = \frac{V(t)}{l}, | J(t) | = \frac{E(t)}{\rho_{layer}} \tag{3}$$

Where $V(t)$ is measured voltage across the HTS tape. The current in each layer can be obtained by integrating the current density over the cross section of each layer. If I_{total} is the total measured current, the current in HTS layer I_{hts} can be obtained as;

$$I_{hts}(t) = I_{total}(t) - \sum_{i=1}^{n_{layer}} I_i^{layer}(t) \tag{4}$$

Knowing the cross section area of the HTS layer, the resistivity of HTS layer ρ_{hts} can be obtained as;

$$\rho_{hts}(I) = \frac{V(t)}{I_{hts}(t)} \times \frac{S_{hts}}{l} \tag{5}$$

The flux flow resistance value can be accurately calculated by substituting equation 5 into equation 2. To verify the validity of this system of equations, a sample of HTS tape was prepared and the critical current values were measured at 77K under self-field conditions using a 1μV criterion. The resulting value was 145A. The sample was then subjected to a finite element simulation (FEM), in which a current pulse with an amplitude of 1.4% of the critical current was applied and the voltage across the layers of the tape was measured. These results were compared to those obtained from a laboratory experiment, as shown in Figure 2. When the transport current exceeds the critical current value, it is distributed among the other metal layers, and the induced voltages across the sample are proportional to the resistivity of

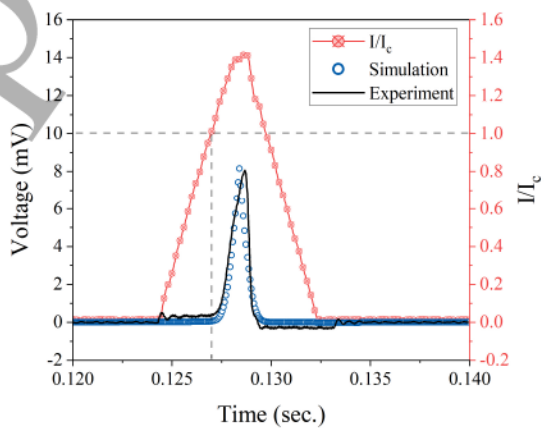

Figure 2: Voltage profile for 8cm long HTS tape measured experimentally and calculated by FEM simulation against normalized applied current (I/I_c).

these layers. Higher currents flowing through the metal layers result in higher voltages, which can facilitate faster charging of the HTS magnet using a self-rectifying flux pump. However, it is important to note that excessive currents can cause quenching of the HTS tape, resulting in heat generation and potentially causing permanent damage to the HTS-CCs. The equations described in this paragraph allow the control block in Figure 1 to estimate the required voltage for injecting flux into the HTS magnet.

2.2. Equivalent Circuit Model

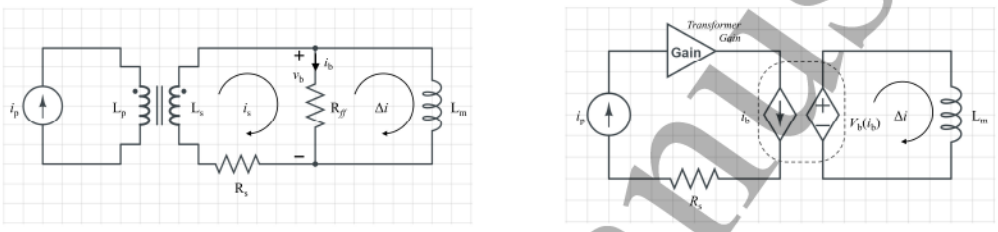

Figure 3: (a) Equivalent circuit diagram of proposed HTS flux pump, R_{ff} in the bridge is flux flow resistivity which only appears when HTS-CC is driven into flux flow regime. (b) Simplified circuit model representing bridge as a current controlled voltage source, transformer is represented by Gain and the solder joint by R_s

To establish a relationship between the primary current (input) and the voltage across the bridge, a simplified magnetic circuit model was developed. When the transport current is below its critical value, the secondary coil is short-circuited by the bridge and the flux flow resistance does not appear. Thus, the load side of the circuit can be neglected under this condition. By applying Kirchhoff's voltage law, the following expressions can be obtained:

$$L_p\frac{di_p}{dt}+M\frac{di_s}{dt}+i_pR_1=0, \tag{6}$$

$$L_s\frac{di_s}{dt}+M\frac{di_p}{dt}+i_sR_s+i_sR_{ff}=0 \tag{7}$$

Where L_p is the inductance of the primary coil, L_s is the inductance of the secondary coil, M is mutual inductance, R_1 is ohmic losses in the primary winding and R_s is the total resistance due to soldering joint in the secondary side. The mutual inductance of the transformer can be regarded as;

$$M=\frac{\phi_c(i_p)}{i_p}, \tag{8}$$

The flux ϕ_c through the transformer core can be calculated by solving the magnetomotive force due to the applied current over the reluctance of the transformer core. Substituting Equation 8 into Equations 6 and 7 yields an expression for the induced current i_s with respect to the applied current i_p. The voltage across the bridge is caused by the flux flow resistivity. By

understanding the relationship between the applied and induced currents, we can represent the flux pump in a simplified circuit diagram by replacing the excitation circuit with a current-controlled voltage source, as shown in Figure 3b. The following equation represents the relationship between the current flowing through the load magnet and the voltage across the bridge caused by flux flow resistivity:

$$\Delta i = \frac{1}{L_m} \int_0^T v_b dt \tag{9}$$

2.3. Applied Current

An asymmetric signal is applied to the primary of the transformer as input. The positive peak has a larger amplitude in order to drive the superconductor into the flux flow regime, while the negative peak has a much lower amplitude in order to maintain the superconducting state. The ratio of the positive period to the negative period is kept inversely proportional to the peak values in order to nullify the dc component. During the positive cycle, the current ramps up to the positive peak I_p at a constant rate and then down to zero at the same rate. Similarly, during the negative cycle, the current ramps down to the negative peak I_n and then up to zero at the same rate. I_p is the amplitude of the positive peak, I_n is the amplitude of the negative peak, i_p is the primary current, and T is the period. These equations are used by the signal generation block in Figure 1 to estimate the required input current for injecting flux into the HTS magnet.

$$\int_0^T i_p(t)\, dt = 0, \tag{10}$$

3. Experiment

The experimental setup, shown in Figure 4, consists of a transformer and a jointless high-temperature superconducting (HTS) magnet. The HTS magnet is made of 12mm-wide, 6m-long YBCO 2G HTS tape with an average critical current of 495A. It was cut longitudinally at its center and wound into a double pancake structure, with each pancake having a width of 6mm and a former diameter of 70mm. One pancake was flipped to align the orientation of the field in the same direction. One side of the jointless HTS coil was extended to form the "bridge". The secondary side of the 300:1 transformer was made of HTS tape with a critical current of 700A, and the terminals were soldered to either side of the bridge, creating the return path for the induced current. The critical current of the bridge is $\leq$248A. Two pre-calibrated current transducers were used to measure the induced voltage on the secondary side and the current in the magnet and provide a feedback signal. A twisted lead voltage tap across the bridge was used to record the voltage. The feedback control was implemented in LabVIEW, with voltage and current readings measured by an NI-9238 DAQ card and the current signal generated by an NI-9263 DAQ card. The power amplifier AE-Techron 7766 was used to generate the primary current for the transformer.

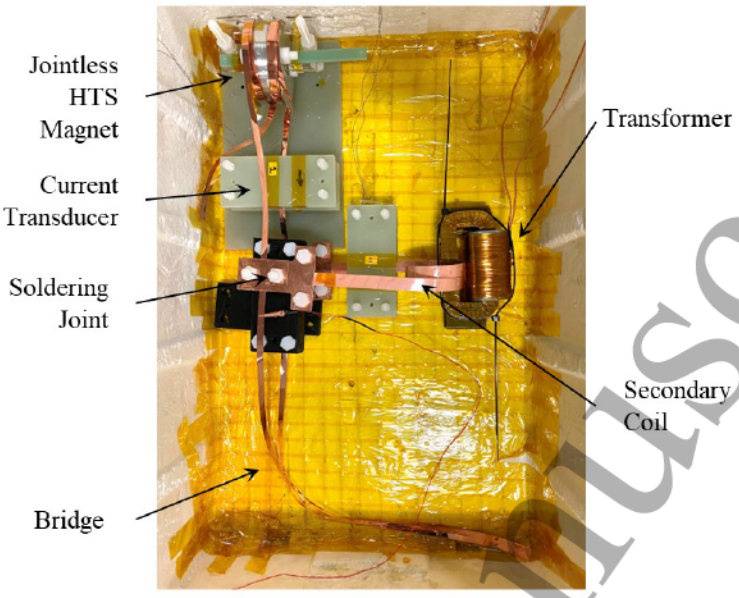

Figure 4: Photograph of proposed flux pump to charge HTS magnet in persistent current operation. Magnet is prepared in jointless fashion and the flux pump is operated in closed-loop feedback control, where a LabVIEW based control calculates the voltage required to inject the required current into the HTS magnet.

3.1. Critical Current of a Jointless HTS Magnet

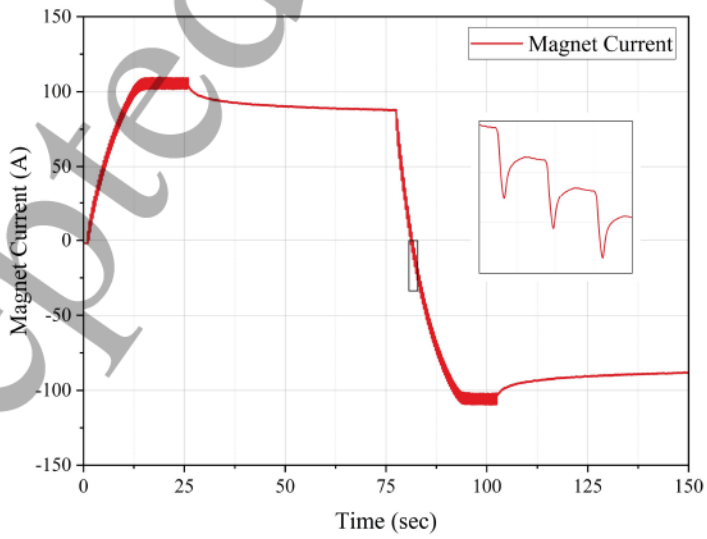

Figure 5: A jointless HTS magnet is charged to it critical current value using a flux pump and the flux pump is switched OFF at time $t = 26sec$, its current decay can be observed due to self field flux creep at critical state and the current stabilizes at 85A.

The preparation of the jointless HTS magnet involves cutting the HTS tape down the

center using mechanical roller blades, which can potentially cause degradation of the critical current due to the mechanical stress applied on the tape [57]. Measuring the critical current of a jointless coil using the four-probe method can be challenging [58], but one approach is to saturate the coil to the point where the phenomenon of flux creep occurs [59]. In HTS coils, there should be no DC losses in theory, but when the coil approaches the critical state, flux flow and flux creep-related losses may occur. The current plot of the jointless magnet used in this study is shown in Figure 5, demonstrating that the magnet saturates at 110A and decays to 85A due to flux creep after the charging is switched off.

3.2. Field Modulation in HTS Magnet Using Closed-Loop Control

The magnetic field of the jointless HTS magnet is modulated by injecting and removing current. The current plot of the HTS magnet is shown in Figure 6. The set point is initially set to 80A. The current in the magnet is zero, so the error is at its maximum. The required voltage for flux pumping is calculated based on the bridge voltage and a primary current signal is generated and sent to the amplifier. This process is repeated continuously until the set point is reached. Once the set point is reached, the required voltage is reduced to zero and the primary signal becomes zero, resulting in the HTS magnet operating in self-field persistent current mode (shown in Figure 6 from time t = 10s to t = 22s). At time t = 22s, a new set point (x = 25A) is assigned and the control block recalculates the voltage required to remove the current from the jointless HTS magnet, generating the corresponding input current signal. At this iteration, the primary current direction is reversed to produce negative voltages across the bridge. The new set point is reached at t = 25s, and the primary signal is switched off, allowing the HTS magnet to operate in persistent current mode. The set point is similarly

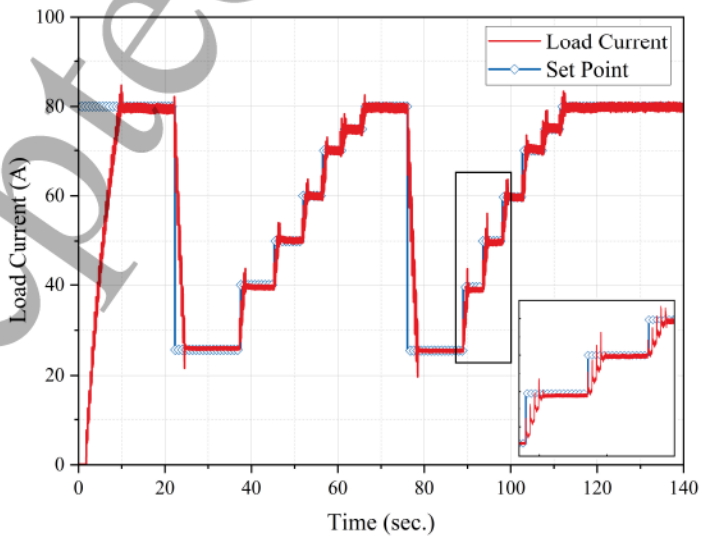

Figure 6: The current in the HTS magnet against the set-point value, the current plot illustrates the field modulation in the HTS magnet and accurate reference tracking in feedback control for a flux pump.

changed to x = 40A, x = 50A, x = 60A, x = 70A, x = 75A, and x = 80A, with the primary current switched off and the HTS magnet operating in persistent current mode after each set point is achieved. The set points are then repeated to validate the accurate operation of the closed-loop feedback control for modulating the HTS magnet's field.

The relation between the charging current (secondary) i_s, the bridge current i_b and the load current Δi can be given as;

$$i_s = i_b + \Delta i, \tag{11}$$

With the increase in the load current, the DC current starts to run through the bridge and the bridge current now has both AC and DC components, due to this a DC biasing in the bridge voltage plot can be seen in Figure 7.

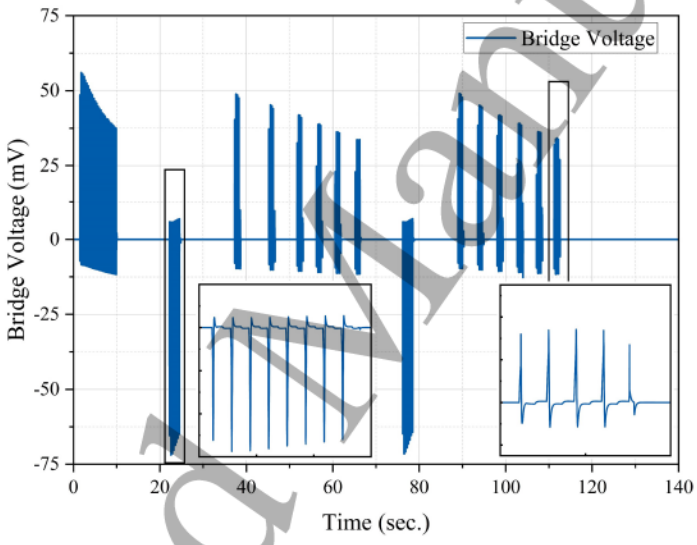

Figure 7: The voltage measured across the bridge during field modulation in HTS magnet.

The charging current plot is shown in Figure 8a. During the first cycle, the charging current is equal to the bridge current since the load current (Δi) is zero. As the load current accumulates, the bridge current becomes biased in the opposite direction. The magnitude of the charging current is automatically adjusted to keep the peak of the bridge current constant in each cycle, as illustrated in Figure 8b. When the load current reaches its set point limit, the input signal returns to zero and the corresponding charging current is also reduced to zero. However, due to the jointless geometry of the HTS magnet, we observe a persistent current flowing in the bridge. Figures 8c and 8d show the charging and discharging cycle of the HTS magnet and its corresponding bridge and charging current in detail. The magnitude of the peaks in the bridge current is nearly constant, indicating the accurate performance of the voltage calculation block in the feedback control.

Closed-loop feedback control is widely used in a variety of applications due to its ability to enable real-time system modification. In this study, we demonstrate the ability to precisely modulate the current of the jointless HTS magnet by 0.5A, as shown in Figure 9a. However, due to the relatively low inductance of the HTS magnet ($\sim$0.5μH), small changes in load

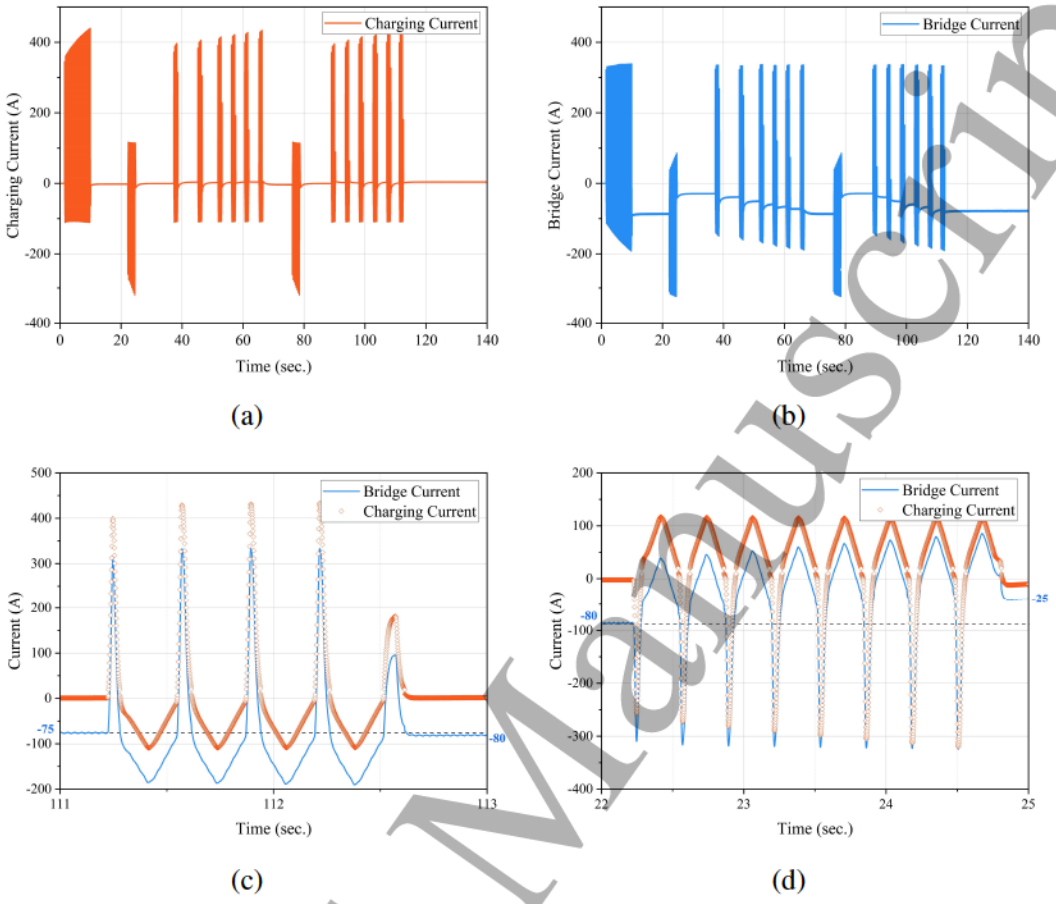

Figure 8: (a) The charging current plot in the HTS secondary side of the transformer. (b) The bridge current plot i_b in HTS flux pump. (c) The bridge current vs charging current plot while charging an HTS magnet by closed loop feedback control operated flux pump. (d) The bridge current vs charging current plot while charging an HTS magnet by closed loop feedback control operated flux pump.

current may not be accurately quantified due to significant ripple noise. Improved precision can be achieved for magnets with higher inductance values. Figure 9b illustrates the induced voltage across the bridge required to inject or remove current from the magnet, which is a step towards developing an ultra-stable DC source for HTS magnets.

4. Discussion and Conclusion

Previous flux pumps have been effective at rapidly increasing currents in large magnets, but they may not be ideal for maintaining field stability. The sharp *V-I* curve of the bridge superconductor makes it difficult to control the bridge voltage effectively, as small variations in the bridge current can cause significant errors in the bridge voltage. This problem has been addressed in previous studies by adding an additional field source perpendicular to the bridge superconductor [24, 25]. However, this solution increases the heat load on the cryogenic

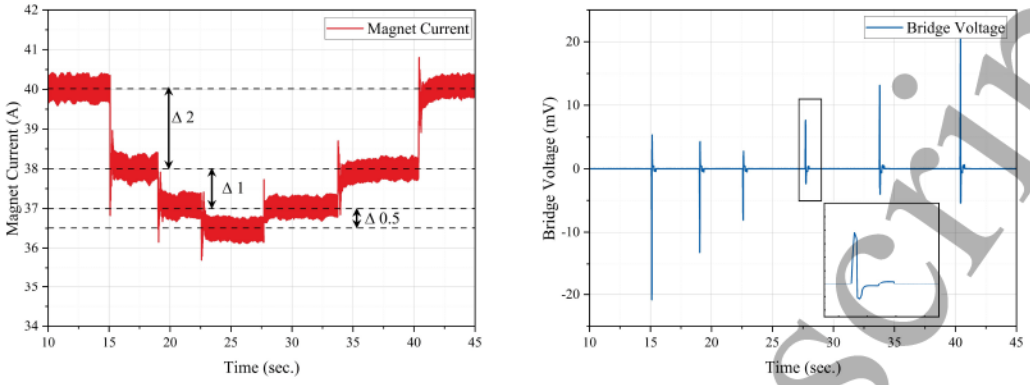

(a) (b)

Figure 9: (a) The current modulation in jointless HTS magnet indicating the precision control by removing the current from the magnet and injecting exactly the same amount. (b) The induced voltages across the bridge to precisely remove and inject the current in an HTS magnet.

system and enlarges its footprint. Moreover, these flux pumps operate using an open loop control. In contrast, the proposed closed-loop control system can provide stable DC voltages on demand, enabling flux pumping at stable DC voltages and achieving persistent current operation in HTS magnets. In theory, a 55 mV voltage can instantly establish an 80 A current in the HTS magnet, but achieving this high voltage in the HTS bridge is only possible in the flux flow regime. In the flux flow regime, the current is shared by other metal layers, which can produce heat and potentially quench the superconductor. Therefore, the superconductor is briefly driven into the flux flow regime to inject current into the magnet. During each cycle, the feedback loop calculates the required voltage and continues injecting current until the set point is reached. The closed-loop feedback control can limit excessive current into the HTS bridge, protecting the system from quenching or overcurrent damage.

We are presenting a closed-loop feedback control system for modulating the magnetic field of high-temperature superconductor (HTS) magnets in persistent current mode. The experimental results demonstrate that this proposed control technique can accurately induce a DC voltage across the HTS bridge, enabling effective flux modulation. In contrast to traditional flux pumps, which do not control the DC voltages across the bridge and rely on the frequency and amplitude of the applied signal for pumping speed, the precision of our flux modulation is demonstrated by the ability to remove a specific current of 0.5A from the magnet on demand. The control block calculates the required voltage of 7mV to generate a corresponding current signal that drives the bridge into the flux flow regime and achieves the desired voltage needed to inject 0.5A. This feedback-controlled flux pump can be used for precise flux modulation of HTS magnets in persistent current operation, addressing the technical challenges associated with using high-current power supplies and current leads and reducing the cooling requirements and footprint of HTS magnets.

Acknowledgement

This work was funded by Prof. Min Zhang Royal Academy of Engineering Research Fellowship. Muhammad H. Iftikhar acknowledges the John Anderson Research Award for offering a fully-funded studentship at the University of Strathclyde, Glasgow, United Kingdom.

References

[1] Parkinson B J, Slade R, Mallett M J and Chamritski V 2012 *IEEE transactions on applied superconductivity* **23** 4400405–4400405
[2] Walsh R M, Slade R, Pooke D and Hoffmann C 2013 *IEEE transactions on applied superconductivity* **24** 1–5
[3] Weijers H, Trociewitz U, Markiewicz W, Jiang J, Myers D, Hellstrom E, Xu A, Jaroszynski J, Noyes P, Viouchkov Y *et al.* 2010 *IEEE transactions on applied superconductivity* **20** 576–582
[4] Iwasa Y 2003 *Cryogenics* **43** 303–316
[5] Hahn S, Park D K, Voccio J, Bascuñán J and Iwasa Y 2011 *Ieee transactions on applied superconductivity* **22** 4302405–4302405
[6] Iijima Y, Kaneko N, Hanyu S, Sutoh Y, Kakimoto K, Ajimura S and Saitoh T 2006 *Physica C: Superconductivity and its applications* **445** 509–514
[7] Freyhardt H C 2007 *International journal of applied ceramic technology* **4** 203–216
[8] Shiohara Y, Yoshizumi M, Izumi T and Yamada Y 2008 *Superconductor Science and Technology* **21** 034002
[9] Liu J, Cheng J and Wang Q 2013 *IEEE transactions on applied superconductivity* **23** 34–39
[10] Ohki K, Nagaishi T, Kato T, Yokoe D, Hirayama T, Ikuhara Y, Ueno T, Yamagishi K, Takao T, Piao R *et al.* 2017 *Superconductor Science and Technology* **30** 115017
[11] Yanagisawa Y, Piao R, Suetomi Y, Yamazaki T, Yamagishi K, Ueno T, Takao T, Ohki K, Yamaguchi T, Nagaishi T *et al.* 2021 *Superconductor Science and Technology* **34** 115006
[12] Lee S, Kim W S, Kim Y, Park S H, Lee J K, Hahn J H, Hong G W, Park I H, Park C and Choi K 2013 *IEEE transactions on applied superconductivity* **23** 4601305–4601305
[13] Ballarino A 2015 *arXiv preprint arXiv:1501.07166*
[14] Wegener L 2009 *Fusion Engineering and Design* **84** 106–112
[15] Ballarino A 2002 *IEEE transactions on applied superconductivity* **12** 1275–1280
[16] Bumby C W, Badcock R A, Sung H J, Kim K M, Jiang Z, Pantoja A E, Bernardo P, Park M and Buckley R G 2016 *Superconductor Science and Technology* **29** 024008
[17] Sung H, Badcock R, Jiang Z, Choi J, Park M and Yu I 2016 *IEEE Transactions on Applied Superconductivity* **26** 1–4
[18] Jeon H, Lee J, Han S, Kim J H, Hyeon C J, Kim H M, Park D, Do Chung Y, Ko T K and Yoon Y S 2018 *IEEE Transactions on Applied Superconductivity* **28** 1–5
[19] Kalsi S S 2011 *Applications of high temperature superconductors to electric power equipment* (John Wiley & Sons)
[20] Van de Klundert L and ten Kate H H 1981 *Cryogenics* **21** 195–206
[21] Van De Klundert L and Ten Kate H 1981 *Cryogenics* **21** 267–277
[22] Oomen M P, Leghissa M, Ries G, Proelss N, Neumueller H W, Steinmeyer F, Vester M and Davies F 2005 *IEEE transactions on applied superconductivity* **15** 1465–1468
[23] Ishmael S, Goodzeit C, Masson P, Meinke R and Sullivan R 2008 *IEEE transactions on applied superconductivity* **18** 693–696
[24] Geng J and Coombs T 2015 *Applied Physics Letters* **107** 142601
[25] Geng J, Matsuda K, Fu L, Shen B, Zhang X and Coombs T 2016 *Superconductor Science and Technology* **29** 035015
[26] Chung Y, Muta I, Hoshino T, Nakamura T and Shon M 2004 *Cryogenics* **44** 839–844

[27] Bai Z, Yan G, Wu C, Ding S and Chen C 2010 *Cryogenics* **50** 688–692
[28] Fu L, Matsuda K and Coombs T 2016 *IEEE Transactions on Applied Superconductivity* **26** 1–4
[29] Hoffmann C, Pooke D and Caplin A D 2010 *IEEE Transactions on Applied Superconductivity* **21** 1628–1631
[30] Coombs T, Fagnard J F and Matsuda K 2014 *IEEE Transactions on Applied Superconductivity* **24** 1–5
[31] Jiang Z, Hamilton K, Amemiya N, Badcock R and Bumby C 2014 *Applied Physics Letters* **105** 112601
[32] Bumby C, Jiang Z, Storey J, Pantoja A and Badcock R 2016 *Applied Physics Letters* **108** 122601
[33] Hildebrandt A F, Wahlquist H and Elleman D D 1962 *Journal of Applied Physics* **33** 1798–1800
[34] Hildebrandt A F, Elleman D D, Whitmore F C and Simpkins R 1962 *Journal of Applied Physics* **33** 2375–2377
[35] Rose-Innes A 1973 *Cryogenics* **13** 103–105
[36] Van Beelen H, AJPT Arnold M, Sypkens H, De Bruyn Ouboter R, Beenakker J and Taconis K 1963 *Physics letters* **7**
[37] Van Suchtelen J, Volger J and Van Houwelingen D 1965 *Cryogenics* **5** 256–266
[38] Atherton D 1968 *Journal of Applied Physics* **39** 2639–2639
[39] Van Beelen H, De Langen M and Kerkdijk C 1969 *Physica* **42** 265–276
[40] Purcell J and Payne E 1961 Superconducting rectifiers *Advances in Cryogenic Engineering* (Springer) pp 149–153
[41] Hempstead C, Kim Y and Strnad A 1963 *Journal of Applied Physics* **34** 3226–3236
[42] Buchhold T 1964 *Cryogenics* **4** 212–217
[43] Geng J and Coombs T 2016 *Superconductor Science and Technology* **29** 095004
[44] Ye H, Wang W, Zhang Y, Li H, Wei J, Xu H, Zhou Q, Liu X and Lei Y 2021 *IEEE Transactions on Applied Superconductivity* **31** 1–5
[45] Zhang Y, Wang W, Ye H, Wang X, Gao Y, Zhou Q, Liu X and Lei Y 2020 *IEEE Transactions on Applied Superconductivity* **30** 1–5
[46] Carroll K 1973 *Cryogenics* **13** 353–360
[47] Vysotsky V, Karasik V, Pechen E, Lebedev P, Markovsky N and Shevchenko O 1990 *Superconductor Science and Technology* **3** 259
[48] Zhai Y, Ma G, Deng Y, Sun C, Li Y and Zhou P 2022 *Cryogenics* 103486
[49] Ali M Z, Zheng J, Huber F, Zhang Z, Yuan W and Zhang M 2020 *Superconductor Science and Technology* **33** 04LT01
[50] Bose B K 1988 *IEEE Transactions on industrial Electronics* **35** 160–177
[51] Steck D A, Jacobs K, Mabuchi H, Bhattacharya T and Habib S 2004 *Physical review letters* **92** 223004
[52] Vijay R, Macklin C, Slichter D, Weber S, Murch K, Naik R, Korotkov A N and Siddiqi I 2012 *Nature* **490** 77–80
[53] Power S Super power inc URL `www.superpower-inc.com/Technology`
[54] Riva N, Richard S, Sirois F, Lacroix C, Dutoit B and Grilli F 2019 *IEEE Transactions on Applied Superconductivity* **29** 1–5
[55] Group H M W Modeling of high temperature superconductors (hts) URL `www.htsmodelling.com`
[56] Zou S, Zermeño V M, Baskys A, Patel A, Grilli F and Glowacki B 2016 *Superconductor Science and Technology* **30** 014010
[57] Liu L, Zhu Y, Yang X, Qiu T and Zhao Y 2016 *IEEE Transactions on Applied Superconductivity* **26** 1–6
[58] Chaudhari P, Koch R, Laibowitz R, McGuire T and Gambino R 1987 *Physical review letters* **58** 2684
[59] Kumar R, Malik S, Pai S, Apte P, Pinto R, Vijayaraghavan R and Kumar D 1992 *Physical Review B* **46** 5766